PCCP
Physical Chemistry Chemical Physics

Accepted Manuscript

This article can be cited before page numbers have been issued, to do this please use: E. M. Gavilán Arriazu, J. M. Hümöller, O. A. Pinto, B. López de Mishima, E. P. M. Leiva and O. A. A. Oviedo, *Phys. Chem. Chem. Phys.*, 2020, DOI: 10.1039/D0CP01886D.

View Article Online
DOI: 10.1039/D0CP01886D

ARTICLE

Fractional and integer stages of lithium ion-graphite systems. The role of electrostatic and elastic contributions.

Received 00th January 20xx,
Accepted 00th January 20xx

DOI: 10.1039/x0xx00000x

E.M. Gavilán-Arriazu[b], J. M. Hümöller[a], O.A. Pinto[b], B.A. López de Mishima[b], E.P.M Leiva[a] and O.A. Oviedo[a]

In the present work we analyze the hot topic of integer and fractional stages lithium-ion batteries by Monte Carlo simulations. While fractional stages have been proposed through several experimental, simulations and theoretical measurements, in other experimental techniques, such as electrochemical ones, there is no evidence for them. In previous work, we have analyzed the thermodynamics and kinetics of lithium-on intercalation using a potential based on empirical parameterization, where multiple stages (integer and fractional) were found and analyzed. The present simulations suggest that, if we consider repulsive elastic interactions in addition to electrostatic ones, the Hamiltonian symmetry is broken and there is no evidence for fractional stages. The physical origin of these repulsive interaction is assigned to the increasing graphite layer separation during lithium-ion intercalation. In the light of these simulations, selected experimental data are revisited, validating the novel parameterization presented. The parametrization used here can be used for other kinds of intercalation compounds, like those involving Na or K.

Keywords: Monte Carlo, lithium-ion battery, graphite, fractional stages, elastic interactions.

1 Introduction

Lithium-ion batteries are today the most commonly used energy storage devices, with graphite being the material preferably employed as the anode electrode. During the lithium-ion loading (intercalations process) and unloading (deintercalation process) in a graphite matrix, it is well known the existence of stable compounds called "stages", which has been detected by different experimental techniques[1–5]. The stages are commonly named as “stage n/m”, which represents the smallest periodic arrangement composed of "m" lithium-ion layers repeated at "n" graphite sheets. When m=1, the stages will be called here “integer” and will be designed with roman numerals (I, II, III, IV, etc.). However, for m>1 the stages are called “fractional”.

In a previous work, we studied the lithium-ion (de)intercalation process in graphite, using Gran Canonical Monte Carlo simulations (GCMC)[6]. In that work, we observed the following sequence of intercalation stages:

$$\mathrm{Id} \rightarrow \mathrm{VIII} \rightarrow \mathrm{IV} \rightarrow \mathrm{III} \rightarrow (\mathrm{III}-\mathrm{II}) \rightarrow \mathrm{II} \rightarrow (\mathrm{II}-3/2) \rightarrow 3/2 \rightarrow 4/3 \rightarrow 8/7 \rightarrow \mathrm{I}\,.$$

This shows the presence of integer and fractional states, and other structures not previously reported, formed by a mixture of integer and fractional ones, like stages $(\mathrm{III}-\mathrm{II})$ and $(\mathrm{II}-3/2)$. While the presence of stage $(\mathrm{III}-\mathrm{II})$ could be caused by the slow convergence of the simulation algorithm, the fractional stages between stages II and I caught our attention for their high symmetry. Particularly, it was highlighted that this symmetry is a consequence of the hole-particle energy symmetry arising from the parameterization (Hamiltonian) used. These fractional stages have been previously reported for Li-ion graphite system by crystallographic and thermodynamic experimental measurements[7,8] and were previously analyzed in other staging works[9–12]. Moreover, the work of Chandesris *et al.*[13] predicts the occurrence of fractional stages using a phase-field model in the staging of graphite intercalation compounds, and explain that the non-occurrence of these stages can be associated with a screening of the repulsive interactions. However, fractional stages are not, or are rarely, observed in most of electrochemical measurements[7,8]. So, regarding the existence of fractional stages, we can advance two possible explanations. In the first place, it could be associated with the presence of "metastable states", which, due to kinetic effects, would allow its measurement[14]. Second, it could be related to the intrinsic description of the interaction potential itself. Whatever the case, the question remains open about which could be the factors that prevent the detection of these structures.

[a] *Instituto de Investigaciones en Fisicoquímica de Córdoba (INFIQC-CONICET), Departamento de Química Teórica y Computacional, Facultad de Ciencias Químicas, Universidad Nacional de Córdoba, Córdoba, Argentina.*
[b] *Instituto de Bionanotecnología del NOA (INBIONATEC). Universidad Nacional de Santiago del Estero (UNSE); CONICET. RN 9, Km 1125. G4206XCP, Santiago del Estero, Argentina.*
** Email: maxigavilan@hotmail.com / o.a.oviedo@unc.edu.ar*
† Footnotes relating to the title and/or authors should appear here.
Electronic Supplementary Information (ESI) available: [details of any supplementary information available should be included here]. See DOI: 10.1039/x0xx00000x

There are different models dealing with the staging of intercalation compounds in graphite. The best known are those from Rüdorff-Hoffman (RH)[15] and Daumas-Hérold (DH)[16]. The RH model considers an ordering of the guest inside the host in such a way that the stages correspond to periodic structure without mismatches consisting of fully-occupied and totally empty layers of guest, as considered in some theoretical models [17,18]. At difference with RH, the DH model assumes that for any stage, all layers are occupied by periodic structure made of clusters of the intercalant. In a previous works[14,19], we have analyzed the topic of RH and DH structures in Li-graphite system from a kinetic viewpoint. We found that RH are expected to be observed at thermodynamics equilibrium, while DH can be considered as frustrated structures, arising due to kinetic factors.

Ion intercalation in graphite is a phenomenon that has been studied for decades, with some kind of compounds as intercalants, especially alkaline metals (Na, K, Li, etc.). A recent compilation work on this thematic can be found in the Reference[20]. It is known that (at least) two possible contributions come into play for stage formation: the electrostatic and elastic interactions[21–23]. The electrostatic interaction is related to the charges of particles, while the elastic is due to the stress produced in the host due to the incremental intercalation process[24]. Some authors have given evidence that elastic interactions induce an expansion of the graphite layers during the intercalation process[10,25]. In the particular case of lithium-ion graphite system, the elastic interaction is mostly caused by the separation of graphite layer due to the increase in the lithium-ion composition[25–29]. The carbon-carbon distances (in the plane of sheets) seems to present negligible modifications compared to the layer separation[30]. Furthermore, there is recent evidence in the work of Mercer *et al*.[31] that during the intercalation process of lithium-ion into graphite, the behaviors of the partial molar entropy at dilute Li-ion compositions can be explained using a model where the Li-C energy is modified with the Li-ion composition, showing the importance of considering the elastic energy effects. We present in **Table 1** the average layer spacing extracted from Reference[30], showing that the separation between the graphite layers varies, depending on the lithium-ion stage. The separation can go up to 11% with respect to free graphite.

Stage	Average graphite layers separation [Å]	Increment in layer separation, Δd [Å]
Graphite	3.35	--------
Id	3.36	$\Delta d_{graphite,Id} = 0.0$
IV	3.45	$\Delta d_{Id,IV} = 0.1$
III	3.47	$\Delta d_{IV,III} = 0.02$
II	3.51	$\Delta d_{III,II} = 0.04$
I	3.73	$\Delta d_{II,I} = 0.22$

***Table 1**. Average graphite layers separation in different stages of Li insertion. Data extracted from Reference[30].*

The largest displacements are around the stage II - stage I transition, this is precisely where most fractional states have been observed. It follows then that it is necessary to consider the effects of the electrostatic and elastic contributions as a function of intercalation percentage. The goal of the present work is emulating the energetic contributions that lead to the graphite layer separation effect using computational methods. It is pertinent to mention that although the stage IIb[4] is present in the reference data used to parametrize our model, we did not have any evidence of this stage in our previous work using GCMC studies[6] and in the preliminary results from the present model. So, we did not consider it for the model parametrization, and so neither in **Table 1**. In fact, the experimental data reveals that the average layer separation is not considerably affected between stages II and IIb (less than 3%), and so can be negligible. We suspect that kinetic factors may be involved in the origin of this kind of diluted intercalation compound, but more experimental and theoretical efforts are necessary to clarify this point.

The article is organized in the following way: section 2, "Computational model", presents details related to the modeling under study, the electrostatic and elastic contributions to the potential energy, and Gran Canonical Monte Carlo methods. In section 3, the results and discussion of simulations are discussed, with special emphasis on the elastic contributions. Finally, section 4 presents the most relevant conclusions.

2 Computational model

2.1. Hamiltonian and Potential Energy Function

To simulate the lithium-ion intercalation process in a graphite matrix, a three-dimensional lattice-gas consisting of K planes of $L \times L$ intercalation sites was used; that is, a total of $M = L \times L \times K$ sites. For simplicity, we consider a AAAA stacking pattern for the graphite matrix. The *x*- and *y*-coordinates of each site of intercalation, correspond to the center of typical hexagonal ring from the graphite "honeycomb" structure. The *z*-coordinate of each intercalation site, corresponds to the middle of two adjacent graphite layer. Therefore, the distance between possible intercalation sites in the same plane is 2.46 Å, while the distance between two sites located one immediately above the other is 3.35 Å. Periodic boundary conditions are imposed in the three exes for approximating a large (infinite) system. We used K = 24, L = 12 and M = 3456 sites.

The model is constructed, as described above, for two reasons. First, to give at Li ions the possibility of formation of compact structures. Second, to consider the energetic equivalent ways formation of √3×√3 layers. Even when the possibility of forming a more compact structure like 1x1 is in principle not excluded, in all simulations Li ions were observed to intercalate at the closest at a distance of √3×2.46 Å in the same plane. **Figure 1** shows the typical simulation cell used, that is, the graphite substrate with Li

intercalation sites, and the typical structure of √3×√3 of lithium in graphite layer. The temperature of system was set to 296 K.

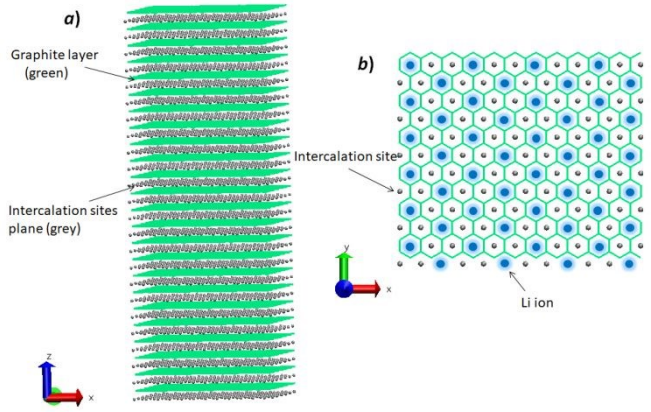

Figure 1. *Simulation cell employed to represent the graphite and Li-intercalation sites. It consists of 48 sites and 24 slab, given a total of 3456 sites of intercalations. a) Side view (x-z plane). b) Top view of the cell (x-y plane) contain a structure of √3×√3 of lithium. Periodic boundary condition in x, y and z directions were applied. Gray and blue spheres correspond to the intercalation site and Li atoms, respectively; Green rings correspond to graphite.*

The Hamiltonian of the system is a variation of that developed by Perassi and Leiva[32], implemented in other works[6,14,19,33,34]. This Hamiltonian contains different electrostatic interactions energy terms, both of them depending on lithium-ion separation distance:

$$H = \frac{1}{2}\sum_{i}^{M}\sum_{j\neq i}^{M^{IP}} c_i c_j E(r_{ij})^{L-J} + \frac{1}{2}\sum_{i}^{M}\sum_{j}^{M^{OP}} c_i c_j E(r_{ij})^{I-I} + \sum_{i}^{M} c_i(\gamma - \mu) \quad (1)$$

where c_i can take the value of 1 if the site *i* is occupied by a lithium, and zero if it is empty. The first term on the *rhs* of equality (1) takes into account the attractive interactions with second neighbors and beyond, while being the interactions to first neighbors repulsive. M^{IP} is a subset of *M* that includes only neighboring sites in the same plane in which *i* is located, with a cutoff radius of 10 Å. This contribution is described by a Lennard-Jones potential,

$$E(r_{ij})^{L-J} = \varepsilon\left[\left(\frac{r_m}{r_{ij}}\right)^{12} - 2\left(\frac{r_m}{r_{ij}}\right)^{6}\right] \quad (2)$$

where ε is the depth of the Lennard-Jones potential at r_m distance. r_{ij} is the distance between *i* and *j* lithium pairs in the same plane. The summation runs over all neighbors up to 10 Å in the *xy* plane (parallel to the graphite layers).

The second summation on the *rhs* of Eq (1) considers repulsive interactions, of electrostatic origin. M^{OP} is other subset of *M*, that considers sites located in planes different from that where site *i* is located, with a cutoff radius of 26 Å. This contribution is modeled by:

$$E(r_{ij})^{I-I} = \kappa\left(\frac{r_b}{r_{ij}}\right)^{\alpha(\theta_k)}\left(1 - e^{-\beta r_{ij}}\right) \quad (3)$$

where κ and r_b are constant parameters. r_{ij} is the distance between *i* and *j* lithium pairs considered now in different planes. The summation runs over all neighbors up to 26 Å in the *z*-axis (this is to consider 7 planes above and below), perpendicular to the graphite layers. The β exponent weakens the repulsive interactions at small distances. The $\alpha(\theta_k)$ coefficient is a function of lithium composition in graphite, where θ_k is the ion lithium composition in graphite for the stage k (θ will be properly defined later), and will be parameterized to take into account experimental elastic interactions. We return to this point in following section.

Finally, the third summation in Eq (1) includes the lithium ion-graphite interaction γ on the surface and the chemical potential μ applied to the Li particles in the simulations. Since we consider pristine graphite, all Li-ion graphite interaction site are energetically equivalent. We present in **Table 2** the Hamiltonian parameter values used in the present work.

Figure 2a shows the plots of the different contributions to the potential energy of interaction of the Li ions in equation (1) using the parameters of **Table 2** and **3**, as a function of the Li-pair distance. The attractive energy contribution, $E(r_{ij})^{L-J}$ in (Eq. 2), shows a potential well of -0.0255 eV, at a distance of 4.26 Å. It increases abruptly for shorter distances, being the reason why Li ions do not form more compact structures. The constant contribution of γ is shown with a red dashed line. The repulsive energy contribution, $E(r_{ij})^{I-I}$ (Eq. 3), with $\alpha(\theta_k)$ = 2.00, is shown as a green curve in **Figure 2a**. Note that this is a pure repulsive energy curve. The elastic contributions are introduced by the changes in $\alpha(\theta_k)$ values. Curves with other colors show $E(r_{ij})^{I-I}$ for $\alpha(\theta_k)$ values of 2.10, 2.12, 2.16 and 2.36, where it can be appreciated how this interaction is reduced as $\alpha(\theta_k)$ increases. **Figure 2b** shows the $\alpha(\theta_k)$ s used for different lattice occupations. Each interval corresponds to a different curve of $E(r_{ij})^{I-I}$ shown in **Figure 2a**. We return to this topic in following sections."

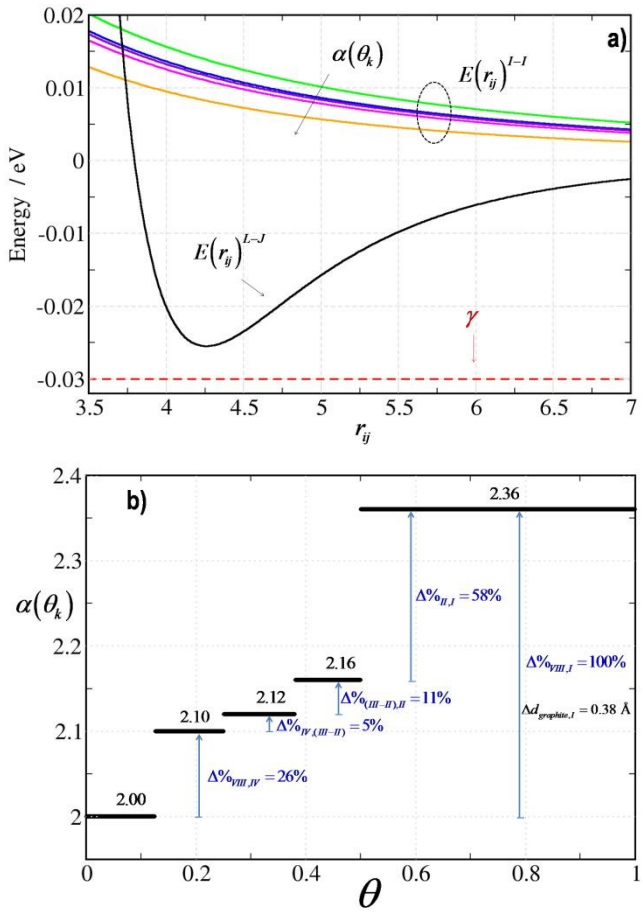

Figure 2. *a) Scheme of the different potential energy contributions as a function of the distance between lithium-ion pairs. While* $E(r_{ij})^{L-J}$ *involves distances measured in the same plane,* $E(r_{ij})^{I-I}$ *correspond to distances in different planes.* γ *is included for comparative purposes. b) Values of* $\alpha(\theta_k)$ *coefficient for different intervals of lithium composition in graphite. The expansion percentage of the graphite sheets,* $\Delta\%_{i,j}$*, is marked in blue, according to the data shown in* ***Table 3****.*

ε[eV]	r_m[Å]	κ [eV]	r_b[Å]	β	γ[eV]
0.0255	4.26	0.255	1.00	1.00	-0.03

Table 2*. Hamiltonian parameters (T=296 K)* [6,32]*.*

2.2. Simulation method

The simulations are performed using the GCMC method [35,36]. The algorithm is based on the Metropolis scheme[37]. Glauber dynamics and a "plane exchange" routine are implemented in order to explore more efficiently the configurational space.

One Monte Carlo Step (MCS) consists in:

- *Step 1*. Given a configuration Ω, a site *i* is randomly chosen between the *M* lattice sites.
- *Step 2*. A new configuration Ω^* is generated, by changing the occupation state of the site *i*.
- *Step 3*.The acceptance probability, $w_{\Omega\to\Omega^*}$, from the transition Ω to Ω^*, is evaluated according to:

$$w_{\Omega\to\Omega^*} = \min\left\{1, \exp\left[-(\Delta U - \mu)/k_B T\right]\right\} \quad (4)$$

where $\Delta U = U(\Omega^*) - U(\Omega)$ is the potential energy difference between the configurations. k_B is the Boltzmann constant and μ is the chemical potential applied to the Li particles in the simulation.

- *Step 4*. Steps 1 to 3 are repeated M times.
- *Step 5*. Given a configuration Γ, a pair of planes *j* and *k* are randomly chosen between the K planes. At least one of them must be occupied by Li ions.
- *Step 6.* A new configuration Γ^* is generated by exchanging the occupation state of the planes *j* and *k*.
- *Step 7*. The acceptance probability, $h_{\Gamma\to\Gamma^*}$, is evaluated according to:

$$h_{\Gamma\to\Gamma^*} = \min\left\{1, \exp\left[-\Delta U / k_B T\right]\right\} \quad (5)$$

where $\Delta U = U(\Gamma^*) - U(\Gamma)$ is the potential energy difference between the configurations.

- *Step 8*. Steps 5 to 7 are repeated K times.

For each temperature and chemical potential, we used an equilibration stage consisting in $1x10^7$ MCS and a processing stage consisting in $1x10^7$ MCS where the variables are averaged.

We should note that as a consequence of the configuration change of step 5 to 7, it may be necessary to update the $\alpha(\theta_k)$ parameter. When there is a stage change, the next steps after the equilibration stage must be performed:

- If the system passes from a stage k to a stage m, then it is necessary to update the coefficient $\alpha(\theta_m) = \alpha(\theta_k) + \Delta\alpha_{k,m}$.
- Recalculate the energy of the system.
- Repeat MCS 1 to 8, according to the equilibration stage.
- Follow to the processing step.

The lithium-ion composition (or intercalation degree) into graphite is calculated as:

$$\theta = \frac{3\langle N\rangle}{M} = \frac{3\sum_i c_i}{M} \quad (6)$$

where $\langle N\rangle$ is the average Lithium number, the number 3 is introduced to ensure standardization of $0 \le \theta \le 1$, since the maximum Li ion composition, in the stage I, is the third part of the total number of sites.

The energy per atom is:

View Article Online
DOI: 10.1039/D0CP01886D

$$U_{Li} = \frac{\langle U \rangle}{\langle N \rangle} \quad (7)$$

where $\langle U \rangle$ is the average potential energy obtained with the Hamiltonian of Eq. (1). The partial molar entropy is:

$$\left(\frac{\partial S}{\partial \theta}\right)_{V,T} = \frac{1}{T}(q_d - \mu) \quad (8)$$

where q_d is the differential heat [38,39], obtained as:

$$q_d = \frac{\langle U\,N \rangle - \langle U \rangle \langle N \rangle}{\langle N^2 \rangle - \langle N \rangle^2} \quad (9)$$

2.3 Parametrization of Li-Li repulsion

We have two alternatives to include the elastic contributions in the simulations. One consists in running simulations varying the size of the simulation box, by increasing the length along the *z*-axis. This allows a relaxation of the graphite planes along this axis, as the intercalation process advances. Given the expansion of the layers, as intercalation proceeds (see **Table 1**), the intercalated lithium-ion in different planes will "feel" less repulsion for being further apart from each other and the potential energy will decrease. Under these conditions it is expected that the isotherms will shift towards lower chemical potentials. In such type of simulations, the repulsive interaction potential between lithium-ions from different planes (Eq. 3) would not be modified.

The second alternative is to modify the repulsive interaction potential between lithium-ions in different planes, in order to introduce the energetic effects of the graphite layers variation without modifying the crystallographic structure of the graphite. This corresponds to decrease the repulsive interaction between ions in different planes as intercalation proceeds. This last alternative has certain advantages over its programming and was the reason why the latter option was chosen. The disadvantage is the need to reparametrize the interaction potential.

The coefficient $\alpha(\theta_k)$ for stage k in Eq. (3) is the key parameter that we will use in the present model to consider the energetic substrate modification upon lithium-ion intercalation. The electrostatic repulsion contribution will be decreased by increasing $\alpha(\theta_k)$. This will mimic the energetic effect observed when the graphite average layer separation increases, when passing from a low to a high composition stage. Under these conditions, lithium-ions will be more separated between them, "feeling" less repulsion between each other.

We can use the increment in layer separation $\Delta d_{i,j}$, corresponding to the change between stages *i* and *j*, upon intercalation (see **Table 1**), to define an expansion percentage $\Delta\%_{i,j}$ as:

$$\Delta\%_{i,j} = 100\frac{\Delta d_{i,j}}{\Delta d_{graphite,I}} \quad (10)$$

where $\Delta d_{graphite,I} = 0.38$ Å is the total change in layer separation from empty graphite to full Li-ion occupation, calculated with the data from **Table 1**.

This parameter will be of great importance to link the layer separation with the energy excess involved in such a change. Let us analyze what this percentage means, and how to link it with the layer separation distance. A value of 100 % in $\Delta\%_{i,j}$ denotes full lithium intercalation, starting from empty graphite. This corresponds to the change in occupation from $\theta = 0.0$ to $\theta = 1.0$. Similarly, the variation between stages II and I, $\Delta\%_{II,I}$, is calculated with the information of **Table 1** as:

$$\Delta\%_{II,I} = 100\frac{\Delta d_{II,I}}{\Delta d_{graphite,I}} = 100\frac{0.22\,\text{Å}}{0.38\,\text{Å}} = 58\% \quad (11)$$

So, $\Delta\%_{II,I} = 58\%$ means that 58% is the change (in percent) of graphite layer average separation when the system goes from stage II to stage I. In the same way, other $\Delta\%_{i,j}$ values can be calculated with Eq. (10) using the $\Delta d_{i,j}$ values of **Table 1**. This information is presented in **Table 3**. Here we also include other parameters of great importance for the present simulations: $\Delta\alpha_{i,j}$ is the change in the coefficient $\alpha(\theta_k)$ when passing from the stage *i* to the stage *j*. This allows following the change of the coefficient during intercalation from the stage *i* to stage *j* as $\alpha(\theta_j) = \alpha(\theta_i) + \Delta\alpha_{i,j}$.

Stages (*i*, *j*)	$\Delta\%_{i,j}$	$\Delta\alpha_{i,j}$	$\alpha(\theta_j)$
graphite, VIII	0 %	0.00	2.00
VIII, IV	26 %	0.10	2.10
IV, III/III-II	5%	0.02	2.12
III-II, II	11%	0.04	2.16
II, I	58 %	0.20	2.36

Table 3*. Energetic parameters obtained from the parameterization.*

We set the initial value $\alpha(\theta_{\text{Id/VIII}}) = 2.0$, for empty graphite and for stages Id and VIII, as used in our previous work considering only electrostatic contributions[6]. The next step is to set up, numerically, the equivalence between the percentage of layer variation $\Delta\%_{i,j}$ and the energetic change that the layer variation produces, *i.e.*, the change $\Delta\alpha_{i,j}$ from a stage to another.

Since we are assuming that the layer separation change between stages I and II, $\Delta d_{graphite,I} = 0.38$ Å, is high enough to break the Hamiltonian symmetry, we search the minimum value of $\Delta\alpha_{II,I}$ such that the system goes from stage II to stage I without the

formation of fractional stages. So, we first run different simulations in this small intercalation interval, parametrizing the equivalence between $\Delta\%_{II,I}$ and $\Delta\alpha_{II,I}$. We chose $\Delta\alpha_{II,I}$ = 0.0, 0.05, 0.10, 0.15 and 2.0 as test values, with an initial value $\alpha(\theta_{II}) = 2.0$.

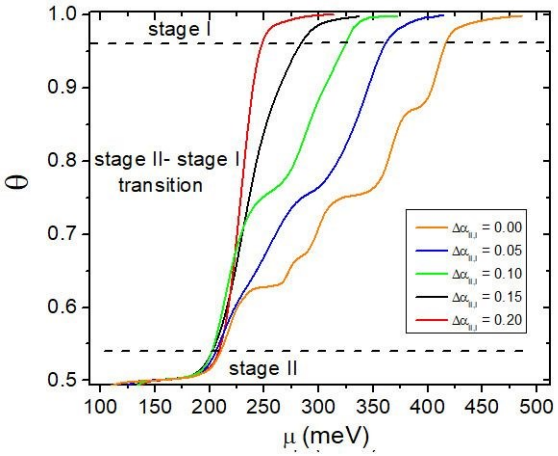

Figure 3. Fractional occupation of the lattice θ as a function of the chemical potential of Li particles μ. The stage II - stage I section of the isotherms obtained with GCMC simulations with different $\Delta\alpha_{II,I}$ values, represented with different colors.

Figure 3 shows the GCMC isotherms obtained for different values of $\Delta\alpha_{II,I}$, where the fractional occupation of the lattice θ is plotted as a function of the chemical potential μ. $\Delta\alpha_{II,I} = 0.0$ (orange line) yields the formation of fractional stages reported in our previous work and does not consider elastic contributions[6]. Multiple stages are found. As $\Delta\alpha_{II,I}$ increases, the fractional states disappear. It can be appreciated that using $\Delta\alpha_{II,I} = 0.20$ is enough to go from the stage $II \rightarrow I$ without intermediate (fractional) structures formed between them, thus breaking the Hamiltonian symmetry. This is evident as a big jump in the transition stage $II \rightarrow I$, marked with dashed lines in **Figure 3**, it is compatible with condensation. For the case $\Delta\alpha_{II,I} < 0.2$ there are indications of plateaus that suggest intermediate configurations in the isotherm curves. Values of $\Delta\alpha_{II,I} > 0.2$ will let go from stage II to stage I without fractional stages. Since we are searching the minimum value for passing from stage II to stage I without fractional stages, we set $\Delta\alpha_{II,I} = 0.2$ for stage $II \rightarrow I$ transitions, as the corresponding value to the percentage of layer variation $\Delta\%_{II,I} = 58\%$. Then, the remaining $\Delta\alpha_{i,j}$ can be deduced from the corresponding $\Delta\%_{i,j}$ from **Table 3** and $\Delta\alpha_{II,I}$. Since stages VIII and (III-II) do not appear in **Table 1**, we assume the same values of $\alpha(\theta_{VIII})$ and $\alpha(\theta_{III-II})$ as those for the previous stages Id and III, respectively. We summarize this information in **Figure 2b**, which shows the intervals values of lithium composition in graphite that we used to emulate the elastic contributions. The $\Delta\%_{i,j}$, are also marked there for a better interpretation. **Figure 4** shows the schematic picture of the change in the separation between graphite layers, which we have used to emulate the elastic effects. Blue spheres correspond to Li ions, while black lines are graphite layers. The intercalation process advances in the direction of the blue arrow. So, as Li ion occupation in graphite increases, the average separation between graphite layers becomes larger(0% for graphite without Li, stages Id and VIII, 26% for stage IV, and so on). The percentage of variation of the interlayer distance, Δ%, between consecutive stages is indicated above and in the middle of the considered stages. The increase in layer separation causes a greater distance between lithium ions in different planes. This decreases the repulsion between them, which is numerically represented in our simulations with an increase in the parameter $\alpha(\theta_k)$.

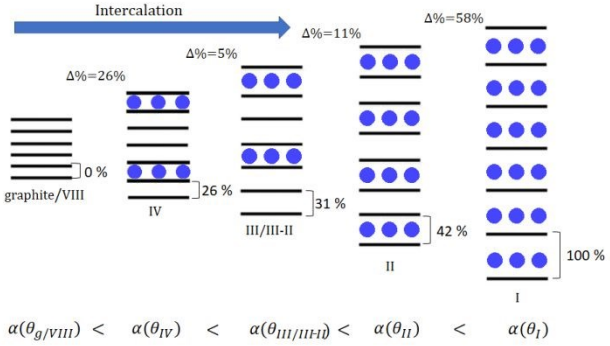

Figure 4. *Schematic picture representing the relationship between graphite layer separation and the energetic parameter $\alpha(\theta_k)$, for each k stage. The blue arrow indicates the progress of intercalation.*

3 Results and discussion

Figure 5 shows θ versus μ for the intercalation process obtained by GCMC simulations with elastic contributions. Starting from the lowest chemical potentials, the stages (indicated by black arrows) appear in the sequence: $Id \rightarrow VIII \rightarrow IV \rightarrow III \rightarrow (III-II) \rightarrow II \rightarrow I$ in a chemical potential window of about 400 meV. The stage sequence is that reported in the literature[2]. Snapshots showing the structure of the stages of **Figure 5** can be observed in **Figure S1a**, from Supplementary Information. Comparison with Figure 4 in reference[6] denotes a greater population of Li ions between the complete sheets. This can be understood in terms of a decreased effective repulsion between ions in different sheets of graphite, due to due to the elastic effects. Likewise, the formation of the √3×√3 ordered structure in the same plane is shown in **Figure S1b** in Supplementary Information.

Figure 6a shows a comparison between the isotherm for $\alpha = 2$ (red dots), i.e., without elastic interactions, and the isotherm for $\alpha(\theta_k)$ having a value for each stage *k* (black line), i.e., with elastic interactions. At first sight, it can be noticed that there is no indication for the occurrence of fractional stages in the black line, as a result of considering the effect of elastic contributions. We must

note that the parameterization was not strong enough to make disappear the other stages previous to stage II, but it was enough to make disappear all the fractional structures. Furthermore, the potential window of the entire intercalation process is smaller in the present model (400 meV) than in our previous work (700 meV). The former value is closer to the experimental potential window[2].

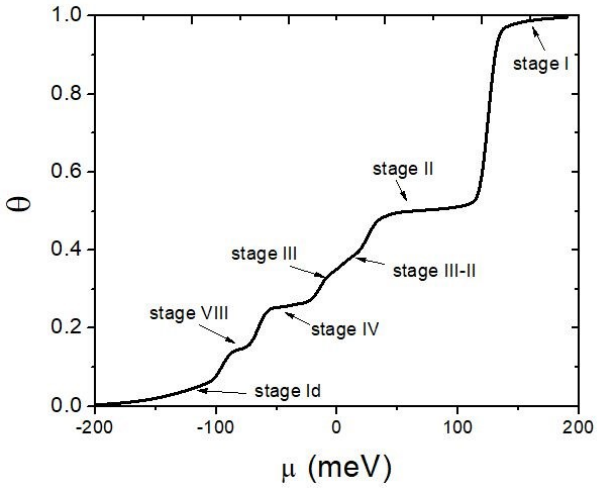

Figure 5. *GCMC simulation results. Lithium ion composition in graphite vs. chemical potential is represented.*

The different contributions to the total potential energy of the system are analyzed in more detail below. This analysis aims to provide understanding on how the decrease in repulsion caused by the elastic interactions operates during the intercalation process. **Figure 6b** shows the energy per atom of Li as a function of the chemical potential with (black line) and without (red dashed line) elastic interactions. It can be seen that for $\mu < -70$ meV, corresponding to the formation of stages Id and VIII, both curves coincide. This is expected, since elastic contributions have not come into play yet (see **Figure 2b**). Both stages are characterized by a significant Li-Li attractive contribution in the same plane and host-guest interactions, evidenced by a sudden change at $\mu \approx -100$ meV towards more negative values in the potential energy per Li atom (stage VIII formation). This sudden change is typical for surface condensation.

The differences begin to be evident upon formation of stage IV. Firstly, it can be seen that the range of chemical potential in which the process takes place, is shorter when considering elastic interactions. Between -60 meV $< \mu < -20$ meV the energy per atom is slightly disturbed by the elastic interactions, since the host deformation is around 0.1 Å ($\Delta\%_{i,j} = 26\%$). Then, in the chemical potential interval -20 meV $< \mu < 0$ meV, formation of stage III begins in the case of consideration of elastic interactions. If the latter are not considered, stage IV is still observed. When stage III is formed, repulsion begins to be important, since the potential energy is increased by the greater repulsion among Li ions in different planes, placed at shorter distances. For $\mu \approx -15$ meV the curve shows an incipient mixture of stages III and II (black curve of **Figure 6a**), which presents practically the same potential energy per atom as stage III (red curve of **Figure 6a**), indicating the importance of considering relaxation of the network.

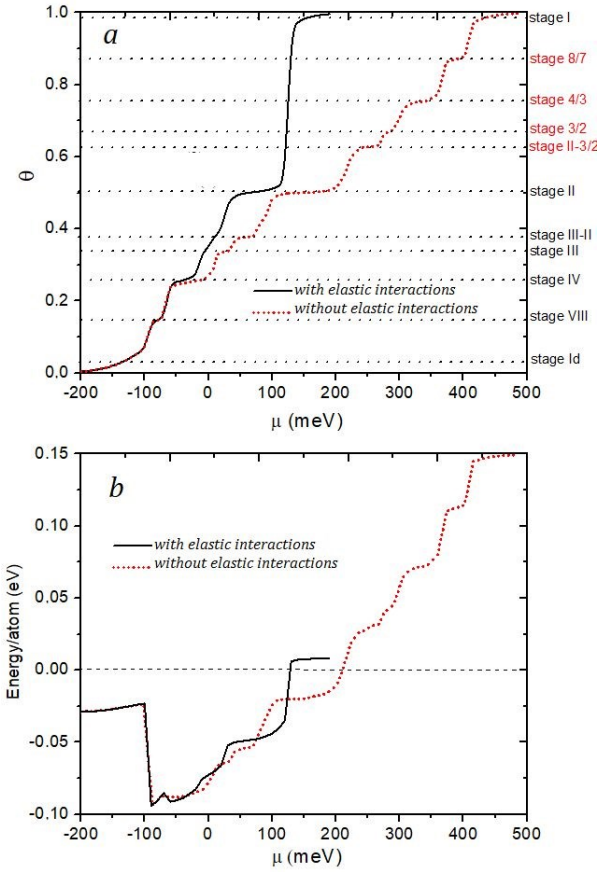

Figure 6. *a) Comparison of lithium composition versus μ with (solid black line) and without (red dotted line) elastic contributions. The stages occupations are marked with dotted lines, and the stages names are detailed on the right hand of the plot. Fractional stages are written with red letters. b) Potential energy per atom for both situations, the curves details are the same as in a).*

In the interval 30 meV $< \mu < 105$ meV, it can be seen that stage II formation takes place when elastic interactions are considered, while this process takes place in the interval 100 meV $< \mu < 200$ meV when these interactions are not considered. The energy per Li atom for stage II with (without) elastic interactions is -50 meV (-25 meV). The percentage of accumulated deformation of the network is 42% (see diagram in **Figure 4**).

Finally, in the intervals 110 meV $< \mu < 190$ meV and 405 meV $< \mu < 490$ meV, the formation of stage I takes places, with and without elastic interactions, respectively. We should point out that only for the stage II-stage I transition there is a difference in the intercalation process. Without the consideration of elastic interactions, the process takes place through a sequence of intermediate fractional states (II-3/2, 3/2, 4/3 and 8/7). On the

other hand, when elastic interactions are considered, state I is formed directly from state II, by a process that resembles condensation. The latter is evidenced by a remarkable increase in the potential energy per Li atom, **Figure 6b**. The energy per Li atom of for stage I with (and without) elastic interactions was 8 meV (150 meV). This large difference in energy is the result of an average increase in the spacing between graphite layers of 0.38 Å, which allows reducing the contributions of the repulsive energy between the ions located in different planes.

It is interesting to compare the present results with experimental data. **Figure 7a** shows $d\mu/d\theta$ *vs* θ. Each peak corresponds to a stage, related to the plateaus of **Figure 5**. While in the present calculations the μ fixed in the GCMC simulation determines θ, in electrochemical systems, this role is played by the electrode potential. In fact, the electrode potential difference, E (difference applied between working and reference electrodes) is linearly related to the chemical potential of the species according to:

$$\mu = C - zeE \tag{12}$$

where z is the number of electrons transferred in the electrochemical reaction, e is the elemental charge and C is a constant that depends on the activity of species in solution and the nature of the reference electrode. The physical reason for the minus sign is due to the fact that, in electrochemistry, an increase of the electrode potential will destabilize the adsorbate, since we are taking away their electrons. Deriving both members of Eq. (12) by Q, we obtain:

$$\frac{d\mu}{dQ} = -ze\frac{dE}{dQ} \tag{13}$$

which shows that the derivative of the chemical potential (obtained from the simulations) is proportional to the derivative of the electrode potential difference (obtained from the electrochemical experiments). This provides a way to compare our simulations with the experimental data reported in References[5,40].

Figure 7a shows the experimental dE/dQ (right axis) and the theoretical $d\mu/d\theta$ (left axis), obtained in our simulations. We note a good correlation between experimental and theoretical predictions, although the stages occupation before stage II are not strictly the same. This is a topic to be investigated in the future, but a priori it could be stated that there is strong evidence that kinetic effects play an important role in the experimental intercalation process, as has been studied in several works[13,14,19,41–43]. This leaves an interesting scenario to study how kinetic effects affect the partial filling of the stages in Li ion-graphite system. The zone in the range $0.5 < \theta < 1.0$ is the transition from stage II to stage I, where it is found that the value of $d\mu/d\theta \to 0$, as observed in experimental measurements. There is evidence that stage III found in experimental measurements (**Figure 7a**, red roman number) is probably stage IV-II, as proposed in the Reference[40]. The occurrence of stage III and I or stage IV-II is another interesting topic that we have addressed previously [6].

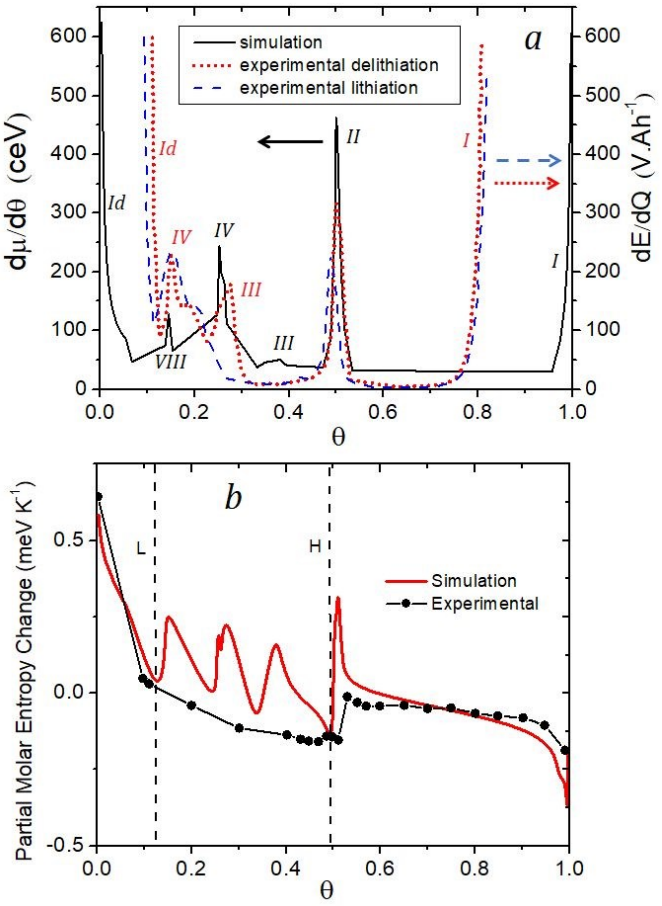

Figure 7. *a)* $d\mu/dQ$ *and* dE/dQ *as a functions of lithium composition in graphite. The black roman numbers indicate the observed stages in simulations and the red roman numbers those from experiments. The black arrow indicates that the left axe data corresponds to the simulation, the blue dashed and the red dotted arrow show that the right data is for experimental data. b) Partial molar entropy vs Li composition in graphite. The experimental information was obtained from Reference*[5,40].

The partial molar entropy changes, obtained in the present simulations according to Eq. (8), is shown in **Figure 7b** (red line) together with its experimental counterpart (black line). The good agreement is clear at low and high occupations $\theta \leq 0.12$ and $\theta \geq 0.5$ (the region marked with an L and H in Figure). However, the partial molar entropy jump at the stage II occupation ($\theta = 0.5$) is higher for simulations. This is expected, since in the theoretical work from Reference[17] it has been remarked that an increase of repulsion interactions of ions placed in different layers would result in higher jumps in molar entropy profiles, and this repulsion is

stronger in simulations. The zone between L and H dashed lines looks different as compared with the experimental case. The simulation shows a series of three maxima that do not appear in the experimental curve. The small number of measurement points in this area make it difficult to argue whether such transitions exist or not.

4 Conclusions

In this paper, we present a way to include elastic contributions into the simulation of an (de)intercalation processes. Although the work is devoted to the understanding of the Li-ion graphite system, it is possible to extrapolate the idea to other compounds. It was possible to obtain several intercalation stages (integer and fractional) and a possible reason why there is no evidence for fractional stages in some measurements was discussed. We present theoretical evidence that the energetic effect of elastic contributions can be responsible for that. The origin of these contributions is the increased host stress upon lithium-ion intercalation. The energetic interpretation of the passage from stage II to stage I without fractional stages is the break of Hamiltonian symmetry (hollow-particle) due to the change in lithium-ion repulsion proposed here. On the other hand, it is remarkable that the Hamiltonian changes did not affect remarkably the formation of integer stages, generally observed in experimental measurements. Simulations were compared with different experimental results to validate the model, showing a reasonable agreement in spite of the simplicity of the model.

Conflicts of interest

There are no conflicts to declare.

Acknowledgements

The authors acknowledges grants PIP CONICET 11220150100624CO, PUE/2017 CONICET, FONCYT PICT- 2015-1605 and SECyT of the Universidad Nacional de Córdoba. Support by CCAD-UNC and GPGPU Computing Group, Y-TEC and an IPAC grant from SNCAD-MinCyT, Argentina, are also gratefully acknowledged. BALM and OAP thanks Universidad Nacional de Santiago del Estero for project CICyT-UNSE 23/A242, Argentina.

The simulations were partially carried out on a HUAUKE parallel cluster located at Instituto de Bionanotecnología del NOA, Universidad Nacional de Santiago del Estero, Santiago del Estero, Argentina.

References

1 M. D. Levi and D. Aurbach, The mechanism of lithium intercalation in graphite film electrodes in aprotic media. Part 1. High resolution slow scan rate cyclic voltammetric studies and modeling, *J. Electroanal. Chem.*, 1997, **421**, 79–88.

2 T. Ohzuku, Y. Iwakoshi and K. Sawai, Formation of Lithium-Graphite Intercalation Compounds in Nonaqueous Electrolytes and Their Application as a Negative Electrode for a Lithium Ion (Shuttlecock) Cell, *J. Electrochem. Soc.*, 1993, **140**, 2490.

3 M. Inaba, H. Yoshida, Z. Ogumi, T. Abe, Y. Mitzutani and M. Asano, In Situ Raman Study on Electrochemical Li Intercalation into Graphite, *J. Electrochem. Soc.*, 1995, **142**, 20.

4 D. Billaud, F. X. Henry, M. Lelaurain and P. Willmann, Revisited structures of dense and dilute stage II lithium-graphite intercalation compounds, *J. Phys. Chem. Solids*, 1996, **57**, 775–781.

5 Y. Reynier, R. Yazami and B. Fultz, The entropy and enthalpy of lithium intercalation into graphite, *J. Power Sources*, 2003, **119–121**, 850–855.

6 E. M. Gavilán-Arriazu, O. A. Pinto, B. A. L. de Mishima, E. P. M. Leiva and O. A. Oviedo, Grand Canonical Monte Carlo Study of Li Intercalation into Graphite, *J. Electrochem. Soc.*, 2018, **165**, A2019–A2025.

7 R. Yazami and Y. Reynier, Thermodynamics and crystal structure anomalies in lithium-intercalated graphite, *J. Power Sources*, 2006, **153**, 312–318.

8 A. Senyshyn, M. J. Mühlbauer, O. Dolotko and H. Ehrenberg, Low-temperature performance of Li-ion batteries: The behavior of lithiated graphite, *J. Power Sources*, 2015, **282**, 235–240.

9 R. Clarke and C. Uher, High pressure properties of graphite and its intercalation compounds, *Adv. Phys.*, 1984, **33**, 469–566.

10 S. A. Safran, Phase Diagrams for Staged Intercalation Compounds, *Phys. Rev. Lett.*, 1980, **44**, 937–940.

11 J. E. Fischer, C. D. Fuerst and K. C. Woo, Staging transitions inintercalated graphite, *Synth. Met.*, 1983, **7**, 1–12.

12 P. Hawrylak and K. R. Subbaswamy, Thermodynamic model of staging transformation in intercalated graphite, *Phys. Rev. B*, 1983, **28**, 4851–4854.

13 M. Chandesris, D. Caliste, D. Jamet and P. Pochet, Thermodynamics and Related Kinetics of Staging in Intercalation Compounds, *J. Phys. Chem. C*, 2019, **123**, 23711–23720.

14 E. M. Gavilán-Arriazu, O. A. Pinto, B. A. López de Mishima, D. E. Barraco, O. A. Oviedo and E. P. M. Leiva, The kinetic origin of the Daumas-Hérold model for the Li-ion/graphite intercalation system, *Electrochem. commun.*, 2018, **93**, 133–137.

15 W. Rüdorff and U. Hofmann, Über Graphitsaelze, *Zeitshrift fur Anorg. und Allg. Chemie*, 1938, **238**, 1–50.

16 N. Daumas and A. Hérold, Notes des Membres et Correspontants et Notes Présentéesou Transmises par Leurs Soins, *C. R. Acad. Sci. Ser. C*, 1969, **268**, 373–375.

17 E. P. M. Leiva, E. Perassi and D. Barraco, Shedding Light on the Entropy Change Found for the Transition Stage II→Stage I of Li-Ion Storage in Graphite, *J. Electrochem. Soc.*, 2017, **164**, A6154–A6157.

18 M. Otero, A. Sigal, E. M. Perassi, D. Barraco and E. P. M. Leiva, Statistical mechanical modeling of the transition Stage II → Stage I of Li-ion storage in graphite. A priori vs

induced heterogeneity, *Electrochim. Acta*, 2017, **245**, 569–574.

19 E. M. Gavilán-Arriazu, O. A. Pinto, B. A. López de Mishima, D. E. Barraco, O. A. Oviedo and E. P. M. Leiva, Kinetic Monte Carlo applied to the electrochemical study of the Li-ion graphite system, *Electrochim. Acta*, 2020, **331**, 135439.

20 Y. Li, Y. Lu, P. Adelhelm, M.-M. Titirici and Y.-S. Hu, Intercalation chemistry of graphite: alkali metal ions and beyond, *Chem. Soc. Rev.*, 2019, **48**, 4655–4687.

21 S. A. Safran and D. R. Hamann, Long-Range Elastic Interactions and Staging in Graphite Intercalation Compounds, *Phys. Rev. Lett.*, 1979, **42**, 3–6.

22 S. Safran and D. Hamann, Electrostatic interactions and staging in graphite intercalation compounds, *Phys. Rev. B*, 1980, **22**, 606–612.

23 S. H. Axdal Anderson and D. D. L. Chung, A Theory fot the Kinetics of Intercalation of Graphite, *Carbon N. Y.*, 1987, **25**, 377–389.

24 M. Gratzel, F. Gutmann, R. R. Haering, S. U. M. Khan, N. Marincic, W. R. McKinnon and O. J. Murphy, *Modern Aspects of Electrochemistry*, Springer US, 1983.

25 J. R. Dahn, Phase diagram of LixC6, *Phys. Rev. B*, 1991, **44**, 9179–9177.

26 E. V. Vakarin and J. P. Badiali, Interplay of configurational and structural transitions in the course of intercalation, *J. Phys. Chem. B*, 2002, **106**, 7721–7724.

27 F. C. Larche and J. W. Cahn, The interaction of composition and stress in crystalline solids., *J. Res. Natl. Bur. Stand. (1934).*, 1984, **33**, 467.

28 Y. Qi, H. Guo, L. G. Hector and A. Timmons, Threefold Increase in the Young's Modulus of Graphite Negative Electrode during Lithium Intercalation, *J. Electrochem. Soc.*, 2010, **157**, A558–A566.

29 B. Xu, M. S. Wu, G. Liu and C. Y. Ouyang, Understanding the effect of the layer-to-layer distance on Li-intercalated graphite, *J. Appl. Phys.*, 2012, **111**, 124325.

30 S. Konar, U. Häusserman and G. Svensson, Intercalation compounds from lih and graphite: Relative stability of metastable stages and thermodynamic stability of dilute stage Id, *Chem. Mater.*, 2015, **27**, 2566–2575.

31 M. P. Mercer, M. Otero, M. Ferrer-Huerta, A. Sigal, D. E. Barraco, H. E. Hoster and E. P. M. Leiva, Transitions of lithium occupation in graphite: A physically informed model in the dilute lithium occupation limit supported by electrochemical and thermodynamic measurements, *Electrochim. Acta*, 2019, **324**, 134774.

32 E. M. Perassi and E. P. M. Leiva, A theoretical model to determine intercalation entropy and enthalpy: Application to lithium/graphite, *Electrochem. commun.*, 2016, **65**, 48–52.

33 E. M. Gavilán Arriazu, B. A. López de Mishima, O. A. Oviedo, E. P. M. Leiva and O. A. Pinto, Criticality of the phase transition on stage two in a lattice-gas model of a graphite anode in a lithium-ion battery, *Phys. Chem. Chem. Phys.*, 2017, **19**, 23138–23145.

34 E. M. Gavilán-Arriazu, M. P. Mercer, O. A. Pinto, O. A. Oviedo, D. E. Barraco, H. E. Hoster and E. P. M. Leiva, Effect of temperature on the kinetics and thermodynamics of electrochemical insertion of Li-ions into a graphite electrode, *J. Electrochem. Soc.*, 2020, **167**, 013533.

35 K. W. Kehr and K. Binder, in *Applcations of Monte Carlo Method in Statistical Physics*, ed. K. Binder, Springer, Berlin, 1987, vol. 36, pp. 181–221.

36 R. L. Strawderman, Monte Carlo Methods in Statistical Physics, *J. Am. Stat. Assoc.*, 2001, **96**, 778–778.

37 N. Metropolis, A. W. Rosenbluth, M. N. Rosenbluth, A. H. Teller and E. Teller, Equation of state calculations by fast computing machines, *J. Chem. Phys.*, 1953, **21**, 1087–1092.

38 O. A. Pinto, B. A. López de Mishima, E. P. M. Leiva and O. A. Oviedo, Monomolecular adsorption on nanoparticles with repulsive interactions: a Monte Carlo study, *Phys. Chem. Chem. Phys.*, 2016, **18**, 14610–14618.

39 O. A. Pinto, B. A. López De Mishima, E. P. M. Leiva and O. A. Oviedo, Simulation of selective thermodynamic deposition in nanoholes, *Phys. Chem. Chem. Phys.*, 2017, **19**, 1601–1609.

40 D. Allart, M. Montaru and H. Gualous, Model of Lithium Intercalation into Graphite by Potentiometric Analysis with Equilibrium and Entropy Change Curves of Graphite Electrode, *J. Electrochem. Soc.*, 2018, **165**, A380–A387.

41 Y. Guo, R. B. Smith, Z. Yu, D. K. Efetov, J. Wang, P. Kim, M. Z. Bazant and L. E. Brus, Li Intercalation into Graphite: Direct Optical Imaging and Cahn-Hilliard Reaction Dynamics, *J. Phys. Chem. Lett.*, 2016, **7**, 2151–2156.

42 S. Krishnan, G. Brenet, E. Machado-charry, D. Caliste, L. Genovese, T. Deutsch and P. Pochet, Revisiting the domain model for lithium intercalated graphite, *Appl. Phys. Lett.*, 2014, **103**, 251904.

43 R. B. Smith, E. Khoo and M. Z. Bazant, Intercalation Kinetics in Multiphase-Layered Materials, *J. Phys. Chem. C*, 2017, **121**, 12505–12523.

View Article Online
DOI: 10.1039/D0CP01886D